Available online at www.sciencedirect.com
SCIENCE DIRECT®
Journal of Solid State Chemistry 178 (2005) 1165–1170
JOURNAL OF SOLID STATE CHEMISTRY
www.elsevier.com/locate/jssc

Subsolidus phase relations in Na_2O–CuO–Sb_2O_n system and crystal structure of new sodium copper antimonate $Na_3Cu_2SbO_6$

O.A. Smirnova[a,b], V.B. Nalbandyan[b,*], A.A. Petrenko[b], M. Avdeev[a]

[a]*Department of Ceramics and Glass Engineering, CICECO, University of Aveiro, 3810-193 Aveiro, Portugal*
[b]*Chemistry Faculty, Department of General and Inorganic Chemistry, Rostov State University, Zorge 7, Rostov-on-Don 344090, Russian Federation*

Received 29 November 2004; received in revised form 31 January 2005; accepted 2 February 2005

Abstract

Subsolidus phase relation studies in the $NaSb_3O_7$–Na_3SbO_4–CuO–$CuSb_2O_6$ quadrangle of Na_2O–CuO–Sb_2O_n system at 1123–1173 K revealed the formation of one new compound $Na_3Cu_2SbO_6$. It is a superstructure derived from α-$NaFeO_2$ type, space group $C2/m$, lattice constants: $a = 5.6759(1)$ Å, $b = 8.8659(1)$ Å, $c = 5.8379(1)$ Å, $\beta = 113.289(1)^\circ$. All ions are in octahedral environment, but CuO_6 polyhedron exhibits strong elongation due to Jahn–Teller effect (Cu–O: 2.000(2) Å × 2, 2.021(2) Å × 2, 2.494(3) Å × 2), whereas SbO_6 octahedron is almost regular. The relationship to other similar superlattices is discussed.

Keywords: Antimonate; Sodium copper antimony oxide; Phase relations; X-ray diffraction; Rietveld refinement; Jahn–Teller effect; α-$NaFeO_2$ type; Superstructure; Pseudosymmetry

1. Introduction

Recently [1–3], we investigated a series of quasi-ternary systems, A_2O–MO–Sb_2O_5 (where A = Na or K, M = Ni, Co, Zn, or Mg) and found several non-stoichiometric layered phases, $A_xM_{(1+x)/3}Sb_{(2-x)/3}O_2$, exhibiting high cationic conductivity. In their structures, $M(2+)$ and Sb(5+) are distributed at random over octahedral sites within brucite-like $(M,Sb)O_{6/3}$ layers. However, partially ordered sodium-containing phases appeared at the stoichiometric compositions, $x = 1$, i.e., $Na_3M_2SbO_6$. In continuation of these studies, we report here the results on the Na_2O–CuO–Sb_2O_5 system, which proved to be quite different.

To our knowledge, phase relations in this ternary system have not been reported in literature to date. In the Na_2O–Sb_2O_5 quasi-binary system, three sodium antimonates (5+) are known: monoclinic Na_3SbO_4 [4], rhombohedral ilmenite type $NaSbO_3$ [5] and orthorhombic $NaSb_5O_{13}$ [6]. However, the last mentioned compound could only be prepared using the hydrothermal method. In the solid-state reaction regime (typically, above 1100 K in air), partial reduction takes place in the antimony-rich compositions, and the system becomes ternary (Na_2O–Sb_2O_5–Sb_2O_3) rather than binary. The cubic pyrochlore type phase, $Na_{1+x}Sb^{3+}_{1-x}Sb^{5+}_2O_{7-x}$, is homogeneous between ca. 24 and 37 mol% Na_2O at 1073–1412 K [7], and Sb_2O_4 (instead of $NaSb_5O_{13}$) appears at lower alkali content. In the CuO–Sb_2O_5 system, two compounds, $CuSb_2O_6$ and $Cu_9Sb_4O_{19}$, are known. The former is stable in air at high temperatures, whereas the latter could only be prepared at an oxygen pressure of 10 bar [8] to avoid formation of $Cu^+_4SbO_{4.5}$ [9]. $CuSb_2O_6$ exhibits monoclinically distorted trirutile structure [10]. Several sodium copper oxides are known (e.g., NaCuO, $NaCuO_2$, $Na_6Cu_2O_6$) but all of them contain either Cu(1+) or Cu(3+). No compounds are reported in the Na_2O–CuO system.

*Corresponding author. Tel.: +7 863 297 5145.
E-mail address: vbn@rsu.ru (V.B. Nalbandyan).

0022-4596/$ - see front matter © 2005 Elsevier Inc. All rights reserved.
doi:10.1016/j.jssc.2005.02.002

2. Experimental

All samples were prepared by conventional solid-state reactions. Reagent-grade sodium carbonate, antimonic acid $Sb_2O_5 \cdot xH_2O$, and $(CuOH)_2CO_3$ were used as starting materials. Sodium carbonate was dried prior to use while the remaining reagents were analyzed gravimetrically (by calcination at 1173 K to give Sb_2O_4 and CuO, respectively) and used for synthesis in air-dried form. To facilitate homogenizing the polyvalent cations, $CuSb_2O_6$ was taken as one of the starting materials. This was prepared at 1373 K and the phase purity verified by XRD. Weighed amounts of powders (2–4 g total mass) were thoroughly mixed with a mortar and pestle, pressed into pellets, calcined at 1023 K to remove volatile components, reground, pressed, fired at 1123 K for 2 h and quenched on a large steel plate to prevent phase changes. Powder diffraction phase analysis was performed using a DRON-2.0 diffractometer with Cu K_α radiation, and the high-temperature treatment was repeated to confirm that phase equilibrium had been attained. Single-phase powder of $Na_3Cu_2SbO_6$ was annealed at 1323 K for 3 h for improved crystallinity and X-ray data were collected using a Rigaku D/Max-B instrument equipped with a secondary beam curved graphite monochromator (Cu K_α radiation, step width 0.02°, counting time 9 s/step). Indexing was performed with the ITO program [11], crystal structure was refined using the FullProf software [12].

3. Results and discussion

3.1. Subsolidus phase equilibria in the Na_2O–CuO–Sb_2O_n system

As mentioned above, reduction to Sb(3+) occurs at the antimony-rich region (>50 mol% Sb_2O_n), whereas preparation of alkali-rich samples (those with Na/Sb ratio greater than three) is complicated by the high volatility of the sodium oxide at elevated temperatures and relatively low melting point of sodium carbonate. Thus, the investigated composition range was limited by the $NaSb_3O_7$–Na_3SbO_4–CuO–$CuSb_2O_6$ quadrangle. In this region, 12 different compositions were prepared and studied. Their powder patterns did not change on repeated firings, even at higher temperature, 1173 K, and not more than three phases were found in each sample; at 1223 K, some mixed-phase samples were melted. These results indicate that equilibrium had been attained at 1123 K and enable partition of the system into phase compatibility triangles (Fig. 1). Only one ternary oxide, $Na_3Cu_2SbO_6$, was identified. In contrast to related Na_2O–MO–Sb_2O_5 systems, where M = Ni, Co, Zn or Mg [1], no solid solution range $Na_x(Cu_{(1+x)/3}Sb_{(2-x)/3})O_2$ could be found. Only the stoichiometric composition, $x = 1$ ($Na_3Cu_2SbO_6$) was homogeneous. At $x<1$, CuO + $NaSbO_3$ appeared, and d spacings of $Na_3Cu_2SbO_6$ remained unchanged.

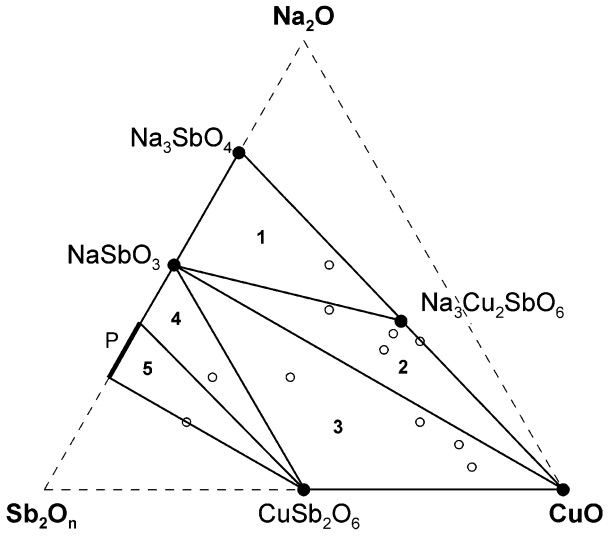

Fig. 1. Subsolidus phase diagram of the Na_2O–CuO–Sb_2O_x system at 1123–1173 K in air. Open circles—mixed-phase samples, filled circles—single-phase samples, P—nonstoichiometric pyrochlore-type sodium antimonate. Phase compatibility triangles: 1—Na_3SbO_4 + $NaSbO_3$ + $Na_3Cu_2SbO_6$; 2—$NaSbO_3$ + $Na_3Cu_2SbO_6$ + CuO; 3—$NaSbO_3$ + CuO + $CuSb_2O_6$; 4—$NaSbO_3$ + P + $CuSb_2O_6$; 5—P + $CuSb_2O_6$.

3.2. Crystal structure of $Na_3Cu_2SbO_6$

$Na_3Cu_2SbO_6$ powder pattern has been completely indexed on a C-centered monoclinic cell (see Table 1) with high figures of merit, $M_{20} = 127$, $F_{30} = 100$, and submitted to the Powder Diffraction File (# 53–342). Reflections with $k \neq 3n$ are scarce and weak indicating a subcell with $b_0 = b/3 = 2.952$ Å. Then, a monoclinically distorted lattice of the α-$NaFeO_2$ type becomes evident. E.g., rhombohedral $Na_{0.8}Ni_{0.6}Sb_{0.4}O_2$ [1,2] may be described in non-standard monoclinic setting with $a = 5.282$, $b = 3.049$, $c = 5.744$ Å, $\beta = 107.85°$. Tripling of the b-axis seems quite natural for $Na_3Cu_2SbO_6$ due to 2:1 ordering of Cu^{2+} and Sb^{5+} ions. Moreover, analysis of the indices has shown that the strongest reflections of $Na_3Cu_2SbO_6$ correspond to strongest lines characteristic of α-$NaFeO_2$ or $Na_{0.8}Ni_{0.6}Sb_{0.4}O_2$, e.g., $(003)_H \rightarrow (001)_M$, $(104)_H \rightarrow (-202)_M + (131)_M$, $(012)_H \rightarrow (200)_M + (-131)_M$, etc. (subscripts H and M refer to the hexagonal subcell and monoclinic supercell, respectively), and even intensities of the split components are approximately proportional to their multiplicity factors.

A realistic model for the structure refinement was, therefore, obtained by transformation of the α-$NaFeO_2$-type atomic coordinates to its superstructure taking into account expected Sb/Cu ordering. In the Rietveld refinement, all space groups permitted by systematic

absences ($C2$, Cm and $C2/m$) were tested; the best quality of fit was obtained for the highest symmetry group, $C2/m$. The refinement details, crystallographic data, atomic parameters and final Rietveld plot are presented in Tables 1 and 2 and Fig. 2. In the starting model, Cu and Sb positions (as well as non-equivalent Na positions) had identical oxygen environment, elongated octahedra. As one can see from interatomic distances (Table 3), refinement resulted in even stronger distortion of the CuO_6 octahedron while the SbO_6 octahedron became almost ideal. These are typical coordinations of Cu^{2+} and Sb^{5+}. Copper has four equatorial oxygens at approximately the same distance 2.0 Å and two more at ~2.5 Å, a characteristic coordination due to the Jahn–Teller effect for the d^9 electron configuration. The four closest oxygens are not, however, strictly coplanar, composing a torsion angle of ca. 17°. This may be ascribed to octahedra stacking conditions. As might be expected, the largest metal–O–metal bond angles (Table 3) are those with higher-valence cation, Sb, and with short Cu–O bonds, due to stronger Coulomb repulsion. Na–O–Na angles are in the range 77–88°.

To further verify the structure, bond valences were calculated according to Brown and Altermatt [13]. As can be seen from Table 4, bond valence sums for anions are in reasonable agreement with their formal valence of two. For cations, however, the situation is complicated: for Cu and Sb, valences are somewhat underestimated, and for Na (especially Na2), overestimated. This correlates with average bond lengths, which, for Cu and Sb (2.172 and 2.045 Å, respectively), are slightly greater than corresponding ionic radii sums (2.13 and 2.00 Å [14]), whereas for Na2–O, the average bond length of 2.351 Å is considerably shorter than ionic radii sum of 2.42 [14]. This might mean partial substitution of Cu for Na and vice versa, but attempts to refine site occupancies showed no Na on Cu site and not more than 5% Cu on Na2 site, which could not explain the above deviations. Similar discrepancies were found for many related structures discussed in the Introduction and in Section 3 below. E.g., the calculated bond valence

Table 1
Crystallographic data, details of the X-ray powder data collection and refinement of the $Na_3Cu_2SbO_6$ structure

Crystal system	Monoclinic
Space group	$C2/m$ (no. 12)
Lattice constants	
a (Å)	5.6759(1)
b (Å)	8.8659(1)
c (Å)	5.8379(1)
β	113.289(1)°
Cell volume (Å^3)	269.8(1)
Formula weight	413.81
Z	2
Density (calc.)	5.093 g/cm^3
2θ range	10–130°
No. of data points	6000
No. of reflections	283
No. of parameters	31
Agreement factors	
R_p	2.36%
R_{wp}	3.28%
R_{Bragg}	3.91%
R_{exp}	1.51%
χ^2	4.72

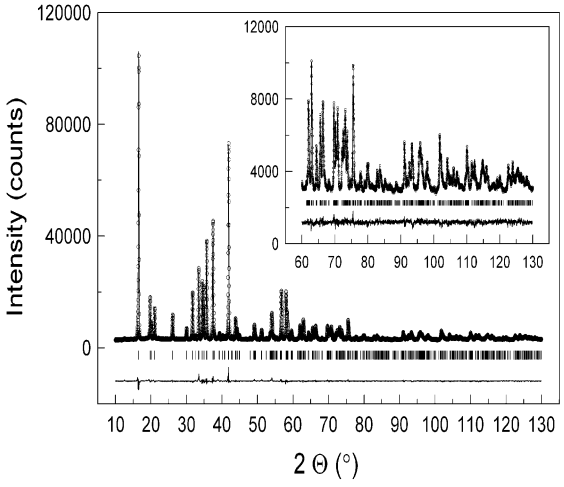

Fig. 2. X-ray diffraction pattern and Rietveld refinement results for $Na_3Cu_2SbO_6$. Observed (circles), calculated (solid line) profiles and difference curve (in the bottom) along with the calculated Bragg peak positions.

Table 2
Atomic coordinates and displacement parameters for $Na_3Cu_2SbO_6$ structure

Atom	Wyckoff position	x	y	z	U_{iso}(Å^2)		
Cu	4g	0	0.6667(1)	0	0.54(3)		
Sb	2a	0	0	0	0.28(3)		
O1	8j	0.2931(4)	0.3340(3)	0.7750(4)	0.45(6)		
O2	4i	0.2404(7)	1/2	0.1774(8)	0.45(6)		
					U_{11}	U_{22}	U_{33}
Na1	2d	0	1/2	1/2	1.1(1)	1.0(1)	0.4(1)
Na2	4h	1/2	0.3280(3)	1/2	$= U_{11}$(Na1)	$= U_{22}$(Na1)	$= U_{33}$(Na1)

Table 3
Selected interatomic distances and bond angles for $Na_3Cu_2SbO_6$ structure

Na1–O1 × 4	2.324(2)	Sb–O1 × 4	2.013(2)	Sb–O1–Cu	94.21(11)
Na1–O2 × 2	2.728(5)	Sb–O2 × 2	2.110(5)		89.81(9)
Na2–O1 × 2	2.301(3)	Cu–O2 × 2	2.000(2)	Cu–O1–Cu	89.60(9)
Na2–O1 × 2	2.335(3)	Cu–O1 × 2	2.021(2)	Sb–O2–Cu × 2	102.22(0)
Na2–O2 × 2	2.418(3)	Cu–O1 × 2	2.494(3)	Cu–O2–Cu	95.27(0)

Table 4
Bond valences and their sums in $Na_3Cu_2SbO_6$ structure calculated according to Brown and Altermatt [13]

	2Na1	4Na2	4Cu	2Sb	ΣV
8O1	0.245	0.260; 0.237	0.397; 0.111	0.825	2.075
4O2	0.082	0.190 × 2	0.420 × 2	0.635	1.937
ΣV	1.144	1.374	1.856	4.570	24.35

sums for sodium are systematically overestimated, namely, 1.17 in $NaSbO_3$ [5], 1.37, 1.30 and 1.08 in Na_3SbO_4 and 1.19, 1.14 and 0.93 in Na_3BiO_4 [4], 1.13 and 1.11 in $Na_3Cd_2IrO_6$ [15], 1.20 and 1.27 in monoclinic Na_2PtO_3, 1.43 and 1.24 in orthorhombic Na_2PtO_3 [16]. These deviations may be due not only to inaccuracy of structural parameters but also to inaccuracy of bond valence parameters. E.g., for regular NaO_6 octahedra, calculation based on these parameters gives bond length of 2.47, sufficiently greater than the sum of octahedral radii [14] and average distances in the above structures. To get correct bond valence sum for octahedral sodium, bond valence parameter R_0 for Na–O bond should be about 1.76 rather than 1.803.

3.3. Comparison with other similar structures

A polyhedral presentation of $Na_3Cu_2SbO_6$ structure together with α-$NaFeO_2$ aristotype [17] is shown in Fig. 3. Both comprise SbO_6, CuO_6 or FeO_6 octahedra, sharing edges to give infinite brucite-like layers, with sodium inserted in distorted octahedral sites between the layers. The two specific features of the former structure are (i) ordering of Sb and Cu on Fe sites, leading to the tripling of the *b*-axis and (ii) strong Jahn–Teller elongation of the CuO_6 octahedron. These differences result in monoclinic rather than rhombohedral symmetry of $Na_3Cu_2SbO_6$.

Many other α-$NaFeO_2$ superlattices of the $A_3M_2LO_6$ formula type are known (in some instances, *A* and *M* or *A* and *L* may be the same element). They belong to the following three structure types:

Li_5ReO_6 [18], $Na_3M_2SbO_6$ (M = Mg, Co, Ni, Zn) [1], $Na_{2.76}Li_{1.24}Ti_2O_6$ [19], Li_2MO_3 (M = Mo, Pd), Na_2MO_3 (M = Hf, Pb) [20], α-Li_2SnO_3 [21], Li_2PtO_3 [22] and high-pressure forms of K_2MO_3 (M = Zr, Hf) [23] seem to be trigonal (proposed space group $P3_112$ or $P3_1$) with parameter *a* (in hexagonal setting) $\sqrt{3}$ that of the aristotype. Another form of Li_5ReO_6, together with $Na_3Cu_2SbO_6$ and five other phases listed at the top of Table 5, belongs to $C2/m$ space group, whereas nine further phases listed at the bottom of Table 5 belong to $C2/c$ space group and have doubled value of the parameter *c* and two layers in the unit cell.

Cation ordering within the brucite layer is the same for all three structure types: each LO_6 octahedron shares edges with six MO_6 octahedra and no LO_6 octahedra, so that *L*–*L* distance is a maximum; the three structure types differ in stacking mode of these identical layers. In the absence of the Jahn–Teller effect, the layers retain almost ideal hexagonal symmetry, which is manifested in the $b/a\sqrt{3}$ ratio being very close to unity (Table 5). Their stacking leads to pseudo-hexagonal metrics of the lattice. To demonstrate this, the second axial ratio, $-(3c\cos\beta)/a$, has been calculated (Table 5). It is equal to unity for ideal hexagonal (or trigonal) lattice and very close to unity for monoclinic phases under consideration, except those containing the Jahn–Teller Cu^{2+} ion.

Monoclinic Li_3RuO_4 [35] exhibits another type of α-$NaFeO_2$ superlattice. Here, the Fe layer is substituted by alternating Ru chains and Li chains, and hexagonal symmetry of the "layer" is completely lost. Nevertheless, pseudohexagonal metrics of the lattice is preserved: $b\sqrt{3}/2a = 0.993$, $-3c\cos\beta/a = 1.028$.

Thus, it is probable that some of the superlattices described as monoclinic might be in fact trigonal [20] and, in turn, some monoclinic phases might be described as trigonal due to either microtwinning/stacking faults or insufficient resolution of powder diffraction patterns. In a recent paper on Na_2RuO_3 [36], two equally good indexing variants, *R*-3*m* and *C*2/*c*, were suggested for the same powder pattern. The authors, however, do not mention weak and broad superlattice features visible at $2\Theta = 19$–20°, incompatible with the small rhombohedral cell and characteristic of superlattices discussed above [1,19,21,22,37].

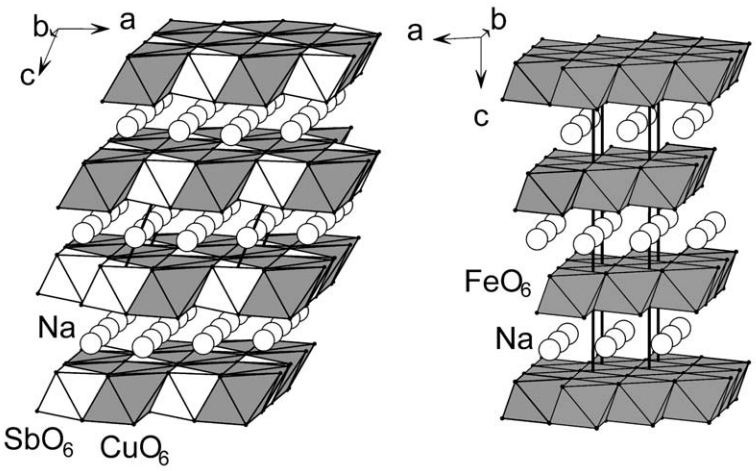

Fig. 3. Polyhedral view of the $Na_3Cu_2SbO_6$ structure (left) in comparison with α-$NaFeO_2$ [17] (right); polyhedra are drawn around copper, antimony and iron atoms, sodium sites are indicated by circles.

Table 5
Cell metrics of different monoclinic ($C2/m$ and $C2/c$) α-$NaFeO_2$ superlattices in comparison with an ideal rhombohedral lattice described in the same setting with tripled b

		$b/a\sqrt{3}$	$(-3c\cos\beta)/a$
Ideal rhombohedral lattice		1	1
$C2/m$	$Li_3Li_2ReO_6$ [24]	0.995	1.028
	$Li_3Zn_2SbO_6$ [25]	0.992	1.036
	$Li_3LiMn_2O_6$ [20]	0.998	1.020
	$Na_3Cd_2IrO_6$ [15]	0.997	1.026
	$Na_3Na_2OsO_6$ [26]	0.991	1.059
	$Na_3Na_2ReO_6$ [24]	0.988	1.060
	$Na_3Cu_2SbO_6$ (this work)	0.902	1.220
$C2/c$	$Li_3LiMn_2O_6$ [27]	1.000	0.964
	$Li_3LiTi_2O_6$ [28]	1.009	1.005
	$Li_3LiRu_2O_6$ [29]	1.029	1.056
	β-$Li_3LiSn_2O_6$ [30]	1.003	1.022
	$Li_3LiPb_2O_6$ [31]	0.999	0.985
	$Na_3NaPt_2O_6$ [16]	1.000	1.003
	$Na_3NaTb_2O_6$ [32]	1.002	1.009
	$K_3NaTh_2O_6$ [33]	0.999	1.007
	$Li_3Cu_2SbO_6$ [34]	0.921	0.477

Strictly speaking, Li_2RuO_3 [29] has *inverse* Li_2TiO_3 structure since Wyckoff positions of tetra- and univalent cations are interchanged, and site symmetry of Ru is different from that of Ti. Nevertheless, coordination and topology are the same, and the compounds are essentially isostructural. On the other hand, $Na_3Cu_2SbO_6$ and $Li_3Zn_2SbO_6$ are, formally, isostructural (since ions with the same oxidation states occupy identical Wyckoff sites with similar fractional coordinates), but exhibit essentially different coordination and should not be considered as completely isostructural.

Ni^{2+}, Co^{2+}, Zn^{2+} and Mg^{2+} are very close to Cu^{2+} in size, but they, together with Sb^{5+}, prefer regular rather than distorted octahedral coordination. As a result, $Na_3M_2SbO_6$ compounds (M = Ni, Co, Zn, Mg) [1] are trigonal rather than monoclinic, exhibit incomplete M/Sb ordering (low intensity of superlattice lines) and permit Sb^{5+} substitution for M^{2+} giving rise to sodium vacancies ($Na_xM_{(1+x)/3}Sb_{(2-x)/3}O_2$) and sodium ion conductivity [1,2], a feature impossible in the system with M = Cu, where no substitution appear (Fig. 1) due to different coordination preferences of Sb^{5+} and Cu^{2+}.

$Li_3Cu_2SbO_6$ [34] differs from $Na_3Cu_2SbO_6$ not only in layer stacking mode resulting in different space group but also in site occupation mode: Li^+ and Cu^{2+} partially substitute for each other on two of the five cation sites, but Na^+ and Cu^{2+} are completely ordered due to size disparity.

4. Conclusions

Subsolidus phase relations in the central part of Na_2O–CuO–Sb_2O_n composition triangle were studied by powder X-ray diffraction after quenching at 1123–1173 K and one new ternary oxide, $Na_3Cu_2SbO_6$, was identified. In contrast to other $Na_3M_2SbO_6$ (M = Ni, Co, Zn, Mg) structures, it is a monoclinic (rather than trigonal) superlattice of the α-$NaFeO_2$ type and does not form cation-conducting sodium-deficient solid solutions, $Na_xM_{(1+x)/3}Sb_{(2-x)/3}O_2$. These differences result from the strong Jahn–Teller distortion of the CuO_6 octahedra which prevents Sb^{5+} substitution for Cu^{2+}. A review of other monoclinic α-$NaFeO_2$ superstructures showed that, in the absence of Jahn–Teller ions, they retain pseudo-hexagonal lattice metrics.

Acknowledgments

Financial support from FCT (Praxis, Portugal, Grant SFRH/BD/6594/2001), RFBR (Russia, Grant 00-03-32469), ICDD (Grant 00-15) and INTAS (Grant YSF-00-125) is greatly appreciated. The authors also thank Dr. V. Kharton for helpful discussions.

References

[1] O.A. Smirnova, V.B. Nalbandyan, V.V. Politaev, L.I. Medvedeva, V.A. Volochaev, I.L. Shukaev, B.S. Medvedev, A.A. Petrenko, in: P. Bezdicka, T. Grygar (Eds.), Solid State Chemistry 2000, September 3–8, Prague, Book of Abstracts, Prague, 2000, p. 228.
[2] O.A. Smirnova, R.O. Fuentes, F. Figueiredo, V.V. Kharton, F.M.B. Marques, J. Electroceram. 11 (2003) 179–189.
[3] O.A. Smirnova, V.B. Nalbandyan, M. Avdeev, L.I. Medvedeva, B.S. Medvedev, V.V. Kharton, F.M.B. Marques, J. Solid State Chem. 178 (2005) 172–179.
[4] B. Schwedes, R. Hoppe, Z. Anorg. Allg. Chem. 393 (1972) 136–148.
[5] B. Wang, S.C. Chen, M. Greenblatt, J. Solid State Chem. 108 (1994) 184–188.
[6] D. Bodenstein, W. Clegg, G. Jäger, P.G. Jones, H. Rumpel, E. Schwarzmann, G.M. Sheldrick, Z. Naturforsch. B 38 (1983) 172–176.
[7] G.M. Kale, S. Srikanth, J. Am. Ceram. Soc. 82 (1999) 2161–2165.
[8] S. Shimada, T. Ishii, React. Solids 7 (1989) 183–186.
[9] M. Stan, S. Mihaiu, D. Crisan, M. Zaharescu, Eur. J. Solid State Inorg. Chem. 35 (1998) 243–254.
[10] A. Nakua, H. Yun, J.N. Reimers, J.E. Greedan, C.V. Stager, J. Solid State Chem. 91 (1991) 105–112.
[11] J.W. Visser, J. Appl. Crystallogr. 2 (1969) 89.
[12] J. Rodriguez-Carvajal, Physica B 192 (1993) 55–69.
[13] I.D. Brown, D. Altermatt, Acta Crystallogr. B 41 (1985) 244–247.
[14] R.D. Shannon, Acta Crystallogr. A 32 (1976) 751–767.
[15] S. Frenzen, Hk. Müller-Buschbaum, Z. Naturforsch. B 51 (1996) 822–825.
[16] W. Urland, R. Hoppe, Z. Anorg. Allg. Chem. 392 (1972) 23–36.
[17] M.S. Goldsztaub, Bull. Soc. France Miner. 58 (1935) 6.
[18] J. Hauck, Z. Naturforsch. B 23 (1968) 1603.
[19] V.B. Nalbandyan, Russ. J. Inorg. Chem. 45 (2000) 1652–1658.
[20] P. Strobel, B. Lambert-Andron, J. Solid State Chem. 75 (1988) 90.
[21] M. Trömel, J. Hauck, Z. Anorg. Allg. Chem. 373 (1970) 8–14.
[22] Powder Diffraction File, JCPDS, 29-820.
[23] C. Delmas, G. Demazeau, M. Devalette, C. Fouassier, P. Hagenmuller, J. Solid State Chem. 19 (1976) 87–94.
[24] T. Betz, R. Hoppe, Z. Anorg. Allg. Chem. 512 (1984) 19–33.
[25] C. Greaves, S.M.A. Katib, Mater. Res. Bull. 25 (1990) 1175–1182.
[26] T. Betz, R. Hoppe, Z. Anorg. Allg. Chem. 524 (1985) 17–25.
[27] A. Riou, A. Lecerf, Y. Gerault, Y. Cudennec, Mater. Res. Bull. 27 (1992) 269–275.
[28] J.F. Dorrian, R.E. Newnham, Mater. Res. Bull. 4 (1969) 179–184.
[29] A.C.W.P. James, J.B. Goodenough, J. Solid State Chem. 74 (1988) 287–294.
[30] J.L. Hodeau, M. Marezio, A. Santoro, R.S. Roth, J. Solid State Chem. 45 (1982) 170–179.
[31] B. Brazel, R. Hoppe, Z. Naurforschung B 38 (1983) 661–664.
[32] R. Wolf, R. Hoppe, Z. Anorg. Allg. Chem. 556 (1988) 97–108.
[33] P. Kroeschell, R. Hoppe, Z. Anorg. Allg. Chem. 509 (1984) 127–137.
[34] J.M.S. Skakle, M.A. Castellanos, S. Trujillo Tovar, A.R. West, J. Solid State Chem. 131 (1997) 115–120.
[35] A. Alexander, P.D. Battle, J.C. Burley, D.J. Gallon, C.P. Grey, S.H. Kim, J. Mater. Chem. 13 (2003) 2612–2616.
[36] K.M. Mogare, K. Friese, W. Klein, M. Jansen, Z. Anorg. Allg. Chem. 630 (2004) 547–552.
[37] J.M. Paulsen, R.A. Donaberger, J.R. Dahn, Chem. Mater. 12 (2000) 2257–2267.